Available online at www.sciencedirect.com
ScienceDirect
Journal of Sound and Vibration 306 (2007) 444–466
JOURNAL OF SOUND AND VIBRATION
www.elsevier.com/locate/jsvi

Impulsive response of an automatic transmission system with multiple clearances: Formulation, simulation and experiment

Ashley R. Crowther[a,*], Rajendra Singh[a], Nong Zhang[b], Chris Chapman[b]

[a]*Acoustics and Dynamics Laboratory, Mechanical Engineering Department, The Ohio State University, 201 West 19th Ave, Columbus, OH 43210, USA*

[b]*Faculty of Engineering, University of Technology, Sydney, PO Box 123, Broadway, NSW 2007, Australia*

Received 22 July 2005; received in revised form 2 October 2006; accepted 4 May 2007
Available online 30 July 2007

Abstract

Impulsive responses in geared systems with multiple clearances are studied when the mean torque excitation and system load change abruptly, with application to a vehicle driveline with an automatic transmission. First, torsional lumped-mass models of the planetary and differential gear sets are formulated using matrix elements. The model is then reduced to address tractable nonlinear problems while successfully retaining the main modes of interest. Second, numerical simulations for the nonlinear model are performed for transient conditions and a typical driving situation that induces an impulsive behaviour simulated. However, initial conditions and excitation and load profiles have to be carefully defined before the model can be numerically solved. It is shown that the impacts within the planetary or differential gears may occur under combinations of engine, braking and vehicle load transients. Our analysis shows that the shaping of the engine transient by the torque converter before reaching the clearance locations is more critical. Third, a free vibration experiment is developed for an analogous driveline with multiple clearances and three experiments that excite different response regimes have been carried out. Good correlations validate the proposed methodology.

1. Introduction

Conditions under which teeth separate and collide in geared systems have fascinated researchers over the last three decades. This is evident from a detailed summary of the existing literature that was conducted by Wang et al. [1]. They examined about 200 papers and found essentially the following two types of problems that arise due to the omnipresent backlashes. First, the gear rattle problem, which manifests itself due to externally applied pulsating torque under light or zero mean operating torques [2,3]. Second, the gear whine problem, which is excited by internal transmission error and/or periodic gear mesh variations at gear mesh frequencies and their harmonics. Nonlinear effects include the jump phenomenon, sub-harmonic resonances and the like [4–6]. Yet, there is another class of problem that was not addressed in Ref. [1]. It deals with impacting gear teeth when the mean operating torque is suddenly changed. In context of vehicle drivelines it is

*Corresponding author.
E-mail addresses: crowther@eng.uts.edu.au (A.R. Crowther), singh.3@osu.edu (R. Singh).

0022-460X/$ - see front matter © 2007 Elsevier Ltd. All rights reserved.
doi:10.1016/j.jsv.2007.05.053

had been dubbed the 'clunk' problem. This paper will illustrate the key features of this problem via an automatic transmission equipped powertrain system with multiple clearances. Theory will be compared with analogous experiments.

2. Problem formulation

Both numerical and semi-analytical methods have been used to examine the typical gear rattle problem [2,7]. Padmanabhan et al. [8] discuss model reduction, numerical stiffness and non-dimensional formulations for gear rattle problems. Kim et al. [9] have assessed four types of smoothening functions for the discontinuous stiffness nonlinearity. Krenz [10] provides perhaps the earliest experimental results for "clunk' in a vehicle driveline, as induced by transient torques and load reversals which also excite the lowest mode of the powertrain (termed as 'shuffle' or 'surging'). Prior researchers have typically focused on modelling gear impacts in manual transmissions and such studies are commonly complimented with rig tests [11–16]. It is evidently a difficult problem as few remedial measures are available. Some suggestions, such as a reduction in the component inertias or in angular speed [12] are difficult to implement. Since the literature on vehicle clunk [11–16] is sparse, a systematic approach is needed to formulate tractable problems. For instance, consider the generic example of Fig. 1 for a geared torsional system with piecewise nonlinear elastic connections (or multiple clearances) as required for the transient excitation problem. Natural modes of this system will vary depending on sub-system separation(s). Our example case of Fig. 2, rear wheel drive vehicle, is installed on a powertrain test rig and is fitted with an automatic transmission (AT) consisting of a torque converter with lock-up clutch, four multi-plate wet clutches, two brake bands, two one-way clutches and a two-staged Ravigneaux planetary gear set. For details such as the powerflow schematic and gear settings, see Ref. [17]. The chief objectives are as follows: (1) Formulate a detailed linear, torsional model of powertrain (with AT) and develop reduced order systems to yield tractable nonlinear problems. (2) Examine nonlinear cases and predict impulsive motions. (3) Validate methodology with experiment. On a more fundamental note, this article will contribute to the transient analysis of geared systems with clearances and stimulate reader interest in contributing to research in transient problems in nonlinear systems.

3. Nature of the transient excitation

A key assumption within this paper is that analysis can be simplified by omitting a torque converter model, in the case of unlocked converter. The nature of the torque excitation, $T_1(t)$, is transient at the engine (due to throttle change) and shaped by the converter fluid coupling before reaching the transmission. To illustrate this, consider a two degree of freedom, first order, semi-definite model with engine inertia, J_1, reflected transmission, driveline and vehicle inertia lumped into J_2, and c_1, a viscous damping element representing the fluid coupling within the torque converter. This system is given by the following equation in terms of $\Omega = \dot{\theta}_1 - \dot{\theta}_2$ with system parameters τ, κ_1, κ_2, where T_2 is a constant vehicle load:

$$\tau\dot{\Omega} + \Omega = \kappa_1 T_1(t) + \kappa_2 T_2,\ \tau = \frac{J_1 J_2}{c_1(J_1 + J_2)},\ \kappa_1 = \frac{J_2}{c_1(J_1 + J_2)},\ \kappa_2 = \frac{J_1}{c_1(J_1 + J_2)}. \quad (1a-d)$$

The analytical solution is $\Omega(t) = \kappa_1 T_{1s} e^{-t/\tau}$, given the ideal step-down excitation at $t = 0$, where $T_{1s} = T_1$ for $t \leqslant 0$, $T_{1s} = 0$ for $t > 0$ and $T_2 = 0$. This expression shows that the rate of change of torque into the transmission system depends on τ and its amplitude is controlled by $\kappa_1(t)$. This is of interest from the standpoint of engine controls and calibration in respect to shaping the transient torque excitation before reaching the clearance locations. One should recognise that an abrupt step-down will not occur in a physical

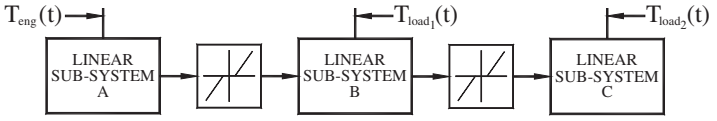

Fig. 1. Generic geared torsional system subject to transient torque excitations. Here the linear sub-systems A–C are joined by the piecewise nonlinear springs (with backlash in the first stage).

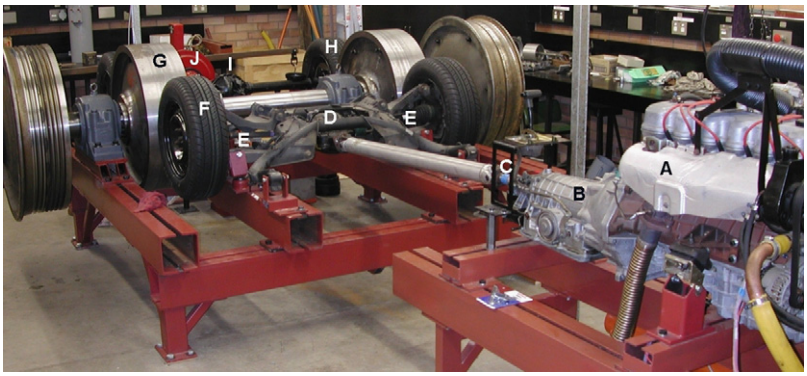

Fig. 2. UTS powertrain test rig (A-engine, B-transmission, C-output shaft strain gauge, D-forward final drive, E-axle strain gauges, F-forward tires, G-flywheels, H-rear tires, I-rear final drive, J-dynamometer).

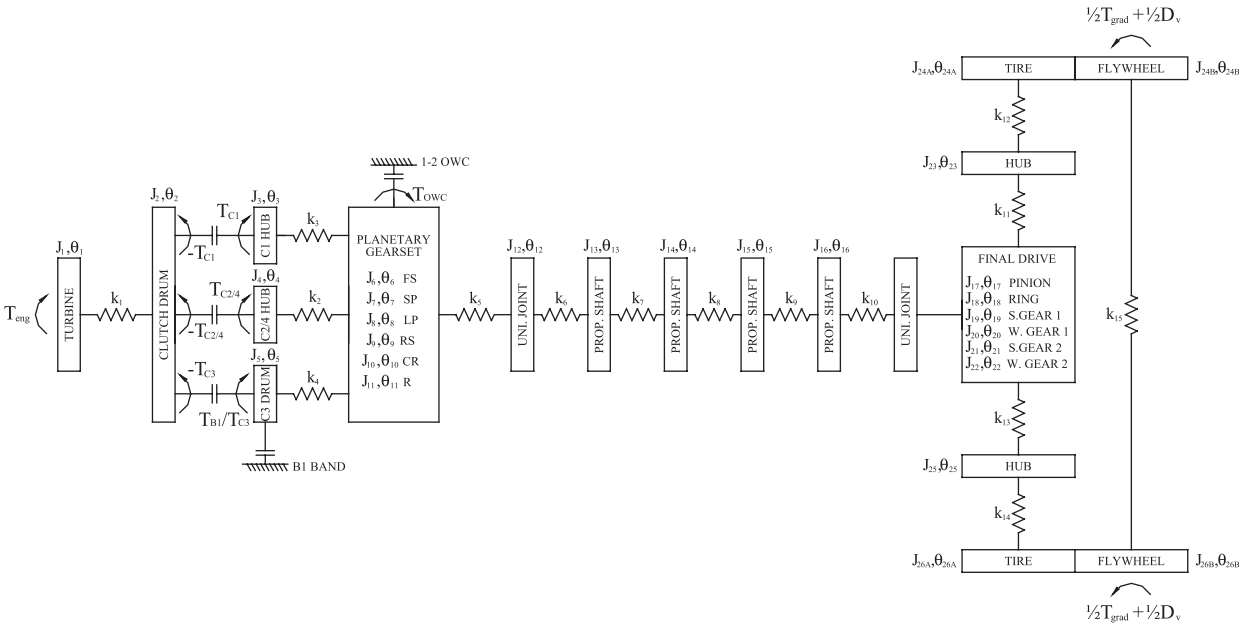

Fig. 3. Detailed lumped torsional model of the automatic transmission powertrain system.

system; a ramp-down is more appropriate to throttle release over a given time span and the sine smoothened ramp-down removes the discontinuous nature of a pure ramp. Given this understanding, the sine smoothened ramp is used as the direct excitation at the turbine, within $T_{\text{eng}}(t)$, in subsequent nonlinear simulations. Mean load and excitation from braking and terrain are also significant to the problem and are included in this study.

4. Detailed model of an automatic transmission powertrain

4.1. Matrix elements for the planetary gear set

A detailed lumped torsional model for the powertrain system is shown in Fig. 3. It may be reduced in various ways and in this paper, two such reductions are made for transient analysis given multiple clearances. Equations of motion for this system are assembled from Newton's laws using lumped matrix elements through the finite element method [18], Lagrangian formulation [19] may be utilised as well. Our approach is also applicable to compounds sets with rigid teeth for analysis of transient gear shifting events [17]. The two-stage gear set (with three planet branches) is modelled using a generalised coordinate vector, $\boldsymbol{\theta} = \{\theta_{\text{fs}}\ \theta_{\text{sp}}\ \theta_{\text{lp}}\ \theta_{\text{rs}}\ \theta_{\text{cr}}\ \theta_r\}^{\text{T}}$,

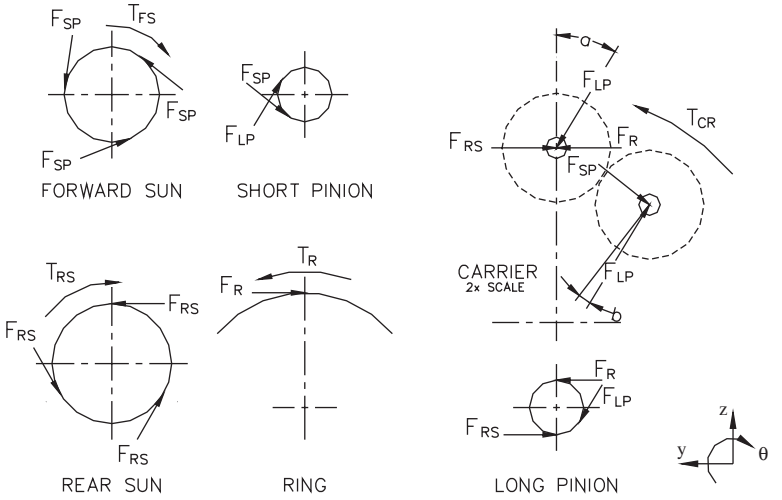

Fig. 4. Free body diagrams of planetary gear set lumped inertias.

where θ_{fs} is the forward sun gear, θ_{rs}, the rear sun gear, θ_{sp} and θ_{lp}, the short and long pinions or planet gears, θ_{cr}, the planet gear carrier that holds the pinions and θ_r, the ring gear. Within the automatic transmission system, the forward sun gear, rear sun gear, planet carrier and ring gear connect through to the clutch drum/propeller shaft via shaft connections. From the free body diagrams of Fig. 4 and considering the motion about gear centerlines we have

$$J_{fs}\ddot{\theta}_{fs} = T_{fs} - 3r_{fs}F_{sp}, \quad 3J_{sp}\ddot{\theta}_{sp} = 3r_{sp}F_{lp} - 3r_{sp}F_{sp}, \tag{2a,b}$$

$$3J_{lp}\ddot{\theta}_{lp} = 3r_{lp}(F_{lp} - F_{rs} - F_r), \quad J_{rs}\ddot{\theta}_{rs} = T_{rs} - 3r_{rs}F_{rs}, \tag{2c,d}$$

$$\begin{aligned} J_{cr}\ddot{\theta}_{cr} &= -T_{cr} + 3(F_{rs} - F_r)(r_{rs} + r_{lp}) + 3F_{sp}(r_{fs} + r_{sp}) - 3F_{lp}(r_{sp} + r_{lp}),\\ J_r\ddot{\theta}_r &= -T_r + 3r_rF_r, \end{aligned} \tag{2e,f}$$

where J and r are each gears inertia and radius and F is the mesh force, given by the tooth bending stiffness and relative displacement. Nomenclature for mesh forces and external torques applied to each gear is indicated in Fig. 4. Acceleration relationships are derived for the gear set via Fig. 5:

$$(a_B)_t = (a_C)_t + (a_{B/C})_t, \quad \ddot{\theta}_{fs}r_{fs} = \ddot{\theta}_{cr}(r_{fs} + r_{sp}) - \ddot{\theta}_{sp}r_{sp}, \tag{3a,b}$$

$$(a_E)_t = (a_F)_t + (a_{E/F})_t, \quad \ddot{\theta}_{rs}r_{rs} = \ddot{\theta}_{cr}(r_{lp} + r_{rs}) - \ddot{\theta}_{lp}r_{lp}, \tag{4a,b}$$

$$(a_G)_t = (a_F)_t + (a_{G/F})_t, \quad \ddot{\theta}_r r_r = \ddot{\theta}_{cr}(r_{lp} + r_{rs}) + \ddot{\theta}_{lp}r_{lp}, \tag{5a,b}$$

$$\frac{(a_F)_t}{\sin e} = \frac{(a_{D/F})_t - (a_{D/C})_t}{\sin c}, \quad \frac{\ddot{\theta}_{cr}(r_{lp} + r_{rs})}{\sin e} = \frac{\ddot{\theta}_{lp}r_{lp} - (-\ddot{\theta}_{sp}r_{sp})}{\sin c} \tag{6a,b}$$

which reduces to

$$\ddot{\theta}_{cr}(r_{lp} + r_{sp}) = \ddot{\theta}_{lp}r_{lp} + \ddot{\theta}_{sp}r_{sp}, \tag{6c}$$

where $(a)_t$ denotes the tangential acceleration of a point on a body with absolute point of reference taken as point A in Fig. 5 or a relative point of reference taken such as point G relative to point F. The acceleration relationships can be used to determine mesh displacement, hence mesh forces, via $F_i = k_i\Delta x_i$ (and by ignoring gear mesh damping), where k designates the mesh stiffness:

$$F_{sp} = k_{sp}\lfloor\theta_{fs}r_{fs} + \theta_{sp}r_{sp} - \theta_{cr}(r_{fs} + r_{sp})\rfloor, \quad F_{lp} = k_{lp}\lfloor-\theta_{lp}r_{lp} - \theta_{sp}r_{sp} + \theta_{cr}(r_{lp} + r_{sp})\rfloor, \tag{7a,b}$$

$$F_{rs} = k_{rs}\lfloor\theta_{lp}r_{lp} + \theta_{rs}r_{rs} - \theta_{cr}(r_{lp} + r_{rs})\rfloor, \quad F_r = k_r\lfloor\theta_{lp}r_{lp} + \theta_{cr}(r_{lp} + r_{rs}) - \theta_r r_r\rfloor. \tag{7c,d}$$

The equations of motion are now formulated with the internal forces replaced by k and Δx and may be assembled to the undamped system $\mathbf{I}\ddot{\boldsymbol{\theta}} + \mathbf{K}\boldsymbol{\theta}(t) = \mathbf{T}(t)$, yielding the matrix elements:

$$\mathbf{I} = \mathrm{diag}[J_{\mathrm{fs}}\ 3J_{\mathrm{sp}}\ 3J_{\mathrm{lp}}\ J_{\mathrm{rs}}\ J_{\mathrm{cr}}\ J_r], \tag{8a}$$

$$\mathbf{K} = \begin{bmatrix} 3r_{\mathrm{fs}}^2 k_{\mathrm{sp}} & 3r_{\mathrm{fs}}r_{\mathrm{sp}}k_{\mathrm{sp}} & 0 & 0 & -3r_{\mathrm{fs}}(r_{\mathrm{fs}}+r_{\mathrm{sp}})k_{\mathrm{sp}} & 0 \\ 3r_{\mathrm{fs}}r_{\mathrm{sp}}k_{\mathrm{sp}} & 3r_{\mathrm{sp}}^2(k_{\mathrm{sp}}+k_{\mathrm{lp}}) & 3r_{\mathrm{sp}}r_{\mathrm{lp}}k_{\mathrm{lp}} & 0 & -3r_{\mathrm{sp}}\left[(r_{\mathrm{fs}}+r_{\mathrm{sp}})k_{\mathrm{sp}}+(r_{\mathrm{sp}}+r_{\mathrm{lp}})k_{\mathrm{lp}}\right] & 0 \\ 0 & 3r_{\mathrm{sp}}r_{\mathrm{lp}}k_{\mathrm{lp}} & 3(r_{\mathrm{lp}}^2k_{\mathrm{lp}}+r_{\mathrm{lp}}^2k_{\mathrm{rs}}+r_{\mathrm{lp}}^2k_r) & 3r_{\mathrm{lp}}r_{\mathrm{rs}}k_{\mathrm{rs}} & 3r_{\mathrm{lp}}\left[-(r_{\mathrm{sp}}+r_{\mathrm{lp}})k_{\mathrm{lp}}-(r_{\mathrm{lp}}+r_{\mathrm{rs}})k_{\mathrm{rs}}+(r_{\mathrm{lp}}+r_{\mathrm{rs}})k_r\right] & -3r_{\mathrm{lp}}r_rk_r \\ 0 & 0 & 3r_{\mathrm{lp}}r_{\mathrm{rs}}k_{\mathrm{rs}} & 3r_{\mathrm{rs}}^2k_{\mathrm{rs}} & -3r_{\mathrm{rs}}(r_{\mathrm{lp}}+r_{\mathrm{rs}})k_{\mathrm{rs}} & 0 \\ -3r_{\mathrm{fs}}(r_{\mathrm{fs}}+r_{\mathrm{sp}})k_{\mathrm{sp}} & -3r_{\mathrm{sp}}\begin{bmatrix}(r_{\mathrm{fs}}+r_{\mathrm{sp}})k_{\mathrm{sp}}\\+(r_{\mathrm{sp}}+r_{\mathrm{lp}})k_{\mathrm{lp}}\end{bmatrix} & 3r_{\mathrm{lp}}\begin{bmatrix}-(r_{\mathrm{sp}}+r_{\mathrm{lp}})k_{\mathrm{lp}}-(r_{\mathrm{lp}}+r_{\mathrm{rs}})k_{\mathrm{rs}}\\+(r_{\mathrm{lp}}+r_{\mathrm{rs}})k_r\end{bmatrix} & -3r_{\mathrm{rs}}(r_{\mathrm{lp}}+r_{\mathrm{rs}})k_{\mathrm{rs}} & 3\begin{bmatrix}(r_{\mathrm{fs}}+r_{\mathrm{sp}})^2k_{\mathrm{sp}}+(r_{\mathrm{sp}}+r_{\mathrm{lp}})^2k_{\mathrm{lp}}\\+(r_{\mathrm{lp}}+r_{\mathrm{rs}})^2k_{\mathrm{rs}}+(r_{\mathrm{lp}}+r_{\mathrm{rs}})^2k_r\end{bmatrix} & -3r_r(r_{\mathrm{lp}}+r_{\mathrm{rs}})k_r \\ 0 & 0 & -3r_{\mathrm{lp}}r_rk_r & 0 & -3r_r(r_{\mathrm{lp}}+r_{\mathrm{rs}})k_r & 3r_{\mathrm{rs}}^2k_r \end{bmatrix} \tag{8b}$$

$$\mathbf{T}(t) = [\,T_{\mathrm{fs}} \quad 0 \quad 0 \quad T_{\mathrm{rs}} \quad -T_{\mathrm{cr}} \quad -T_r\,]^{\mathrm{T}}. \tag{8c}$$

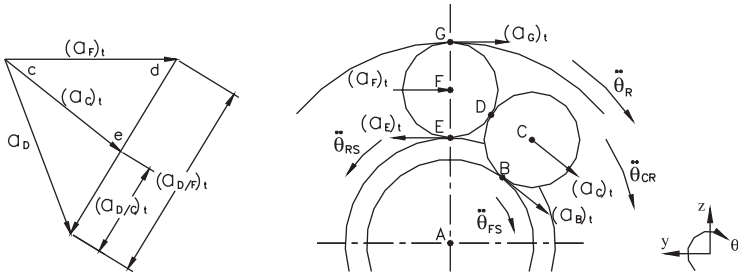

Fig. 5. Acceleration relationships of planetary gear set lumped inertias.

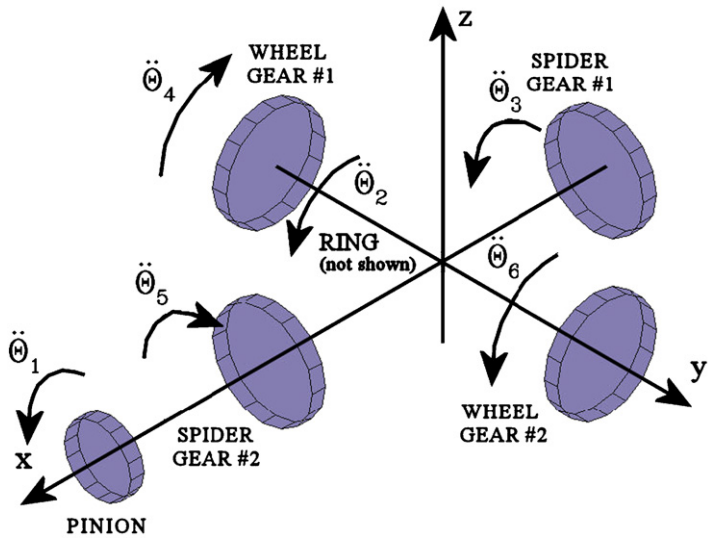

Fig. 6. Final drive and differential lumped coordinates in exploded assembly.

The inertia, **I** and stiffness, **K** matrices are analogous to those from torsional finite elements [17,20]. If these matrix elements are part of a surrounding system then the components of the torque vector Eq. (8c) can be replaced by the torsional stiffness elements that couple the subsystems. This dynamic system has interesting eigenvalue properties which vary depending on constraints imposed. For an unconstrained system, four real eigenvalues are found representing natural frequencies with corresponding modes, two zero eigenvalues are found with eigenvectors that can be combined in a linear combination to find a mode for rigid body motion for a particular gear ratio (i.e. when constrained for a fixed gear). With one constraint applied, e.g. rear sun gear held for second gear, there are again four natural frequencies and now just one rigid body mode (for a particular gear ratio). The natural frequencies and modes can change significantly for the various constraints.

4.2. Matrix elements for the final drive

The final drive (hypoid gear set of Fig. 6) is modelled using the generalised coordinate vector $\boldsymbol{\theta} = \{\theta_1\ \theta_2\ \theta_3\ \theta_4\ \theta_5\ \theta_6\}^{\mathrm{T}}$, where θ_1 is the final drive pinion, θ_2, the ring gear, θ_3 and θ_5, the differential spider gears, θ_4 and θ_6, the differential wheel gears (or side axle gears). Within the driveline, the pinion connects to the propeller shaft and the wheel gears connect to left and right axles. By applying the same methodology as for the planetary gear set the matrix elements are obtained as

$$\mathbf{I} = \mathrm{diag}[J_1\ J_2\ J_3\ J_4\ J_5\ J_6], \tag{9a}$$

$$\mathbf{K} = \begin{bmatrix} r_1^2 k_{12} & -r_1 r_2 k_{12} & 0 & 0 & 0 & 0 \\ -r_1 r_2 k_{12} & r_2^2 k_{12} + r_{2A}^2 (k_{34} + k_{36} + k_{45} + k_{56}) & -r_{2A} r_3 k_{34} + r_{2A} r_3 k_{36} & -r_{2A} r_4 k_{34} - r_{2A} r_4 k_{45} & r_{2A} r_5 k_{45} - r_{2A} r_5 k_{56} & -r_{2A} r_6 k_{36} - r_{2A} r_6 k_{56} \\ 0 & -r_{2A} r_3 k_{34} + r_{2A} r_3 k_{36} & r_3^2 k_{34} + r_3^2 k_{36} & r_3 r_4 k_{34} & 0 & -r_3 r_6 k_{36} \\ 0 & -r_{2A} r_4 k_{34} - r_{2A} r_4 k_{45} & r_3 r_4 k_{34} & r_4^2 k_{34} + r_4^2 k_{45} & -r_4 r_5 k_{45} & 0 \\ 0 & r_{2A} r_5 k_{45} - r_{2A} r_5 k_{56} & 0 & -r_4 r_5 k_{45} & r_5^2 k_{56} + r_5^2 k_{45} & r_5 r_6 k_{56} \\ 0 & -r_{2A} r_6 k_{36} - r_{2A} r_6 k_{56} & -r_3 r_6 k_{36} & 0 & r_5 r_6 k_{56} & r_6^2 k_{36} + r_6^2 k_{56} \end{bmatrix}, \tag{9b}$$

$$\mathbf{T}(t) = [T_1\ 0\ 0\ -T_4\ -T_6]^{\mathrm{T}}. \tag{9c}$$

4.3. Global System Assembly

For the dynamic model of Fig. 3 the global coordinate vector is $\boldsymbol{\theta} = \{\theta_1 \ldots \theta_{26}\}^{\mathrm{T}}$, corresponding to $\mathbf{I}\ddot{\boldsymbol{\theta}} + \mathbf{K}\boldsymbol{\theta}(t) = \mathbf{T}(t)$. This system is assembled from shaft elements for stiffness connections k_1 to k_{14} and the planetary gear and final drive matrix elements. Additionally in assembly, for the planetary gear set, the local coordinate vector is renumbered as $\boldsymbol{\theta} = \{\theta_6, \theta_7, \theta_8, \theta_9, \theta_{10}, \theta_{11}\}^{\mathrm{T}}$ and is used with matrix elements (Eqs. (8a) and (8b)). For the final drive, the local coordinate vector is renumbered as $\boldsymbol{\theta} = \{\theta_{17}, \theta_{18}, \theta_{19}, \theta_{20}, \theta_{21}, \theta_{22}\}^{\mathrm{T}}$ and is used with Eqs. (9a) and (9b). The following should be noted for clarity: (1) The C1 clutch hub and planet carrier are coordinates 3 and 10 for the carrier shaft element, k_3. (2) The C2/4 clutch hub and forward sun gear are coordinates 4 and 6 for the forward sun gear shaft element, k_2. (3) The C3 drum and rear sun gear are coordinates 5 and 9 for the rear sun gear shaft element, k_4. (4) The ring gear and upper universal joint are coordinates 11 and 12 for the output shaft element, k_5. (5) The single piece propeller shaft is divided into five stiffness elements, k_6–k_{10} with mass lumped on the six surrounding coordinates, 12–17. (6) Left and right differential wheel gears (coordinates 20 and 22) connect through the axle stiffness elements, k_{11} and k_{13}, to the wheel hubs (coordinates 23 and 25). As noted later in Section 6, large flywheels on the test rig act as the equivalent mass of a vehicle. Thus, the tire coordinates, θ_{24} and θ_{26}, are connected by the stiff flywheel shaft as shown in the test rig photograph (Fig. 2). The stiff flywheel shaft constrains any differential action except in the vibration mode. The matrix elements for the flywheel shaft, k_{15}, are as follows where r_{tire}, is the tire rolling radius, r_{fly}, is the radius of the flywheels that are in contact with the tire and n_{eff}, the effective 'gear' ratio of these contacting bodies:

$$\boldsymbol{\theta}_{e15} = \begin{Bmatrix} \theta_{24} \\ \theta_{26} \end{Bmatrix} \mathbf{I}_{e15} = n_{\mathrm{eff}}^2\, \mathrm{diag}[J_{24B}\ J_{26B}],\ \mathbf{K}_{e15} = \begin{bmatrix} n_{\mathrm{eff}}^2 k_{15} & -n_{\mathrm{eff}} k_{15} \\ -n_{\mathrm{eff}} k_{15} & n_{\mathrm{eff}}^2 k_{15} \end{bmatrix},\ n_{\mathrm{eff}} = \frac{r_{\mathrm{tire}}}{r_{\mathrm{fly}}}. \tag{10a–d}$$

4.4. Eigensolutions of the linear system

Once assembled, the eigenvalue problem for the system matrix will yield several rigid body modes. Constraints need to be applied to simulate the clutch and band elements. For example, with reference to Table 1, for the transmission in second gear, the C2 clutch is engaged and the B1 brake band is held. Thus in the system of equations of motion, coordinates 2 and 4 are combined and coordinate 5 is grounded. The spider gears are also grounded, so as to model the differential slip clutch locked. Given the above constraints, the real eigensolutions yield one zero eigenvalue and 21 real eigenvalues, which are influenced by a combination of torsional stiffness of the shafts and flexural stiffness at tooth contact. Selected natural frequencies are given in Table 2. The eigenvector corresponding to the zero eigenvalue describes the absolute displacements including ratios for transmission second gear and the final drive.

Table 1
Constrained/engaged coordinates for the detailed model of the automatic transmission powertrain system

Gear	Ratio	Constrained coordinate(s)	Description	Engaged co-ordinate(s)	Description	dof
1st	2.393	10	Carrier held by one way 1–2 clutch	2 and 4	Clutch drum and C2/4 clutch hub engaged	24
2nd	1.480	5	C3 drum held by B1 brake band	2 and 4	Clutch drum and C2/4 clutch hub engaged	24
3rd	1.000	—		2 and 4 2 and 3	Clutch drum and C2/4 clutch hub engaged and C1 clutch hub engaged	24
4th	0.677	5	C3 drum held by B1 brake band	2 and 3	Clutch drum and C1 clutch hub engaged	24
Spider gears grounded	As per gear	19 and 21	Spider gears grounded for no differential action	—	—	22

In all cases spider gears grounded for no differential slip.

4.5. Clearance models

Clearances may be modelled using the piecewise nonlinear stiffness as follows where δ_i, represents the backlash for the ith mesh stiffness element:

$$k_i = \begin{cases} k_i, & |x_i| \geq 0.5\delta_i, \\ 0, & |x_i| < 0.5\delta_i. \end{cases} \tag{11}$$

For a gear pair $x_i = r_i\theta_i \pm r_{i+1}\theta_{i+1}$ is the relative displacement between contacting teeth, where θ is the angular displacement and r the contact radius. The sign is chosen as positive if the gears provide a reversal in direction of rotation and negative if they do not. For the planetary set, the relative displacements are provided within Eq. (7) and for the final drive they may be extracted from Eq. (9b). With the gear mesh force, F, modelled as such, a torque vector is needed to account for the offset of force from the zero position. Thus the global torque vector includes the local torque offsets as

$$T_{\delta(i)} = 0.5\text{sign}(x_i)r_i k_i \delta_i;\ T_{\delta(i+1)} = -0.5\text{sign}(x_i)r_{i+1}k_i\delta_i. \tag{12}$$

Typical locations of clearances include splines (at some shaft connections), within joints (which could be represented in this model by k_6 and k_{10}, for the two universal joints), in multi-staged clutch dampers and in gear sets. Fig. 7 is a typical reduced model that could include clearances in forward sun/short pinion mesh, rear sun/long pinion mesh and long pinion/ring mesh for the planetary gear set. The final drive is represented by pinion and ring gears with yet another clearance in this mesh. The inclusions of all these nonlinearities will pose computational challenges [8] and thus several pragmatic choices must be made to pre-condition the associated numerical stiffness issues: (1) Lump short and long pinions to one coordinate, thereby reducing degrees of freedom by one and removing the highest eigenvalue. (2) Reduce the gear mesh stiffness artificially by 10–100 times, leading to a drastic reduction in the eigenvalue range without greatly changing system response for transient impacts. (3) Carefully select smoothening functions for the discontinuous stiffness functions [9]. (4) Rescale the time variable for a longer solution domain. (5) Further reduce the system order for a particular analysis objective. Within this paper, the last option is chosen for the sake of illustration.

5. Reduced model for automatic transmission powertrain and nonlinear simulation

5.1. Formulation

Fig. 8 presents the reduced order model of the powertrain system with ten degrees of freedom, $\bar{N} = 10$. Note that the tires (and vehicle equivalent inertia) are modelled as a single inertia, $J_{10} = J_{\text{tire}} + r_{\text{tire}}^2 m_v$, where J_{tire} is

Table 2
Mode shape comparison for automatic transmission powertrain system: detailed model versus reduced order model

Mode	Rigid body mode		Driveline shuffle		Axle left		Axle right		Transmission and driveline I	
Natural frequencies (Hz)	**0**	0	**6.54**	6.41	**32.3**	32.1	**33.2**	33.0	**142**	137
Turbine	**1.00**	1.00	**1.00**	1.00	**−0.19**	−0.18	**−0.13**	−0.12	**−0.08**	−0.09
Clutch drum	**1.00**	1.00	**0.98**	0.99	**−0.09**	−0.08	**−0.05**	−0.05	**0.80**	0.76
Transmission driving gears	**1.00**	1.00	**0.97**	0.97	**−0.03**	−0.03	**−0.01**	−0.02	**1.00**	0.96
Transmission driven gears	**0.68**	0.68	**0.66**	0.66	**−0.02**	−0.01	**0.00**	0.00	**0.69**	0.70
Universal joint	**0.68**	0.68	**0.64**	0.63	**0.07**	0.08	**0.06**	0.06	**0.84**	0.86
Final drive pinion	**0.68**	0.68	**0.61**	0.60	**0.18**	0.18	**0.13**	0.13	**1.00**	1.00
Final drive ring	**0.20**	0.20	**0.18**	0.18	**0.06**	0.06	**0.04**	0.04	**0.29**	0.29
Right hub	**0.20**	0.20	**0.05**	0.05	**0.24**	0.25	**1.00**	1.00	**−0.01**	0.00
Left hub	**0.20**	0.20	**0.05**	0.04	**1.00**	1.00	**−0.25**	−0.26	**0.00**	0.00
Tire	**0.20**	0.20	**−0.01**	−0.01	**0.00**	0.00	**0.00**	0.00	**0.00**	0.00

Mode	Transmission and driveline II		Transmission II		Propeller shaft I		Propeller shaft II		Transmission III	
Natural frequencies (Hz)	**250**	247	**532**	476	**1404**	1195	**1759**	1709	**2503**	2114
Turbine	**0.02**	0.02	**0.00**	0.00	**0.00**	0.00	**0.00**	0.00	**0.00**	0.00
Clutch drum	**−0.54**	−0.57	**−0.35**	−0.48	**0.00**	0.00	**0.00**	0.00	**−0.01**	0.00
Transmission driving gears	**−0.30**	−0.33	**1.00**	0.95	**−0.09**	−0.04	**0.06**	−0.02	**1.00**	1.00
Transmission driven gears	**−0.18**	−0.16	**0.74**	1.00	**−0.04**	−0.04	**0.01**	0.00	**−0.50**	0.55
Universal joint	**0.37**	0.39	**0.39**	0.46	**1.00**	1.00	**−0.83**	−0.85	**0.13**	−0.13
Final drive pinion	**1.00**	1.00	**−0.16**	−0.30	**0.07**	0.02	**1.00**	1.00	**−0.01**	0.06
Final drive ring	**0.30**	0.30	**−0.06**	−0.11	**−0.04**	−0.05	**−0.22**	−0.16	**0.00**	0.00
Right hub	**0.00**	0.00	**0.00**	0.00	**0.00**	0.00	**0.00**	0.00	**0.00**	0.00
Left hub	**0.00**	0.00	**0.00**	0.00	**0.00**	0.00	**0.00**	0.00	**0.00**	0.00
Tire	**0.00**	0.00	**0.00**	0.00	**0.00**	0.00	**0.00**	0.00	**0.00**	0.00

Bold values designate reduced model; other values are for detailed model.

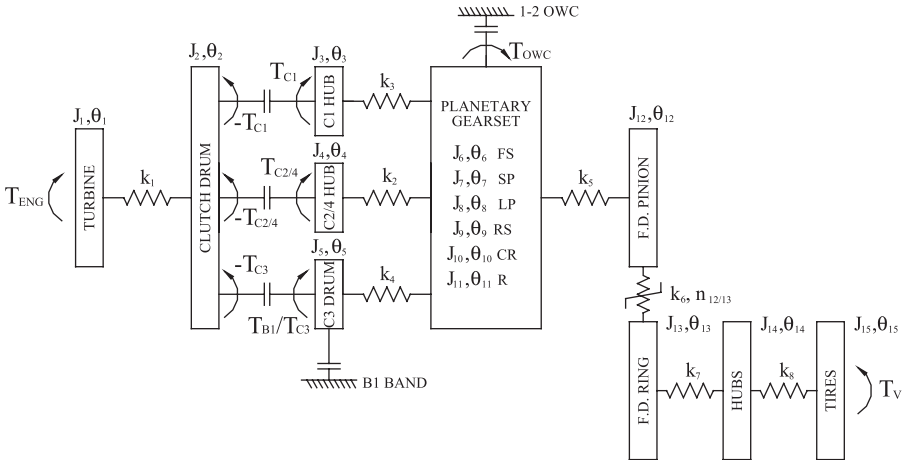

Fig. 7. Reduced order torsional model of automatic transmission powertrain system. This includes unlocked torque converter and clearances in the planetary and final drive gear sets.

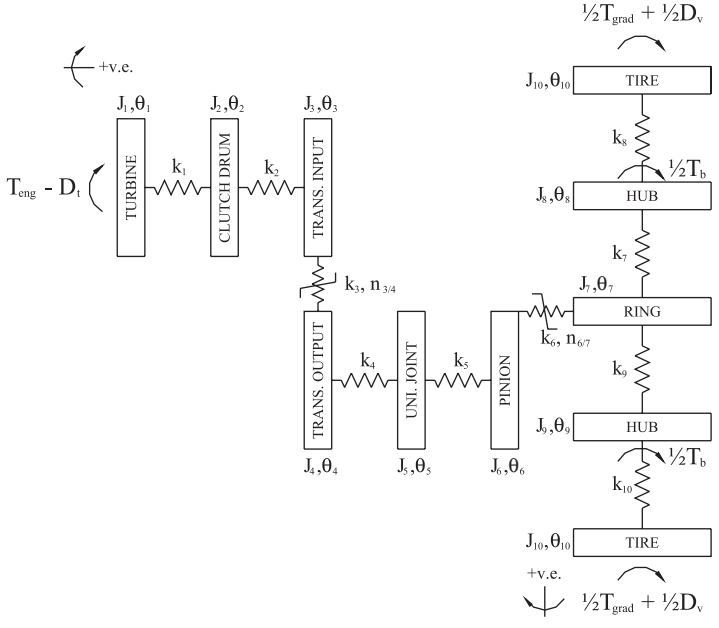

Fig. 8. Reduced order torsional model of automatic transmission powertrain system. This includes unlocked torque converter for fixed gear transient analysis with clearances in transmission and final drive gear pairs.

the tire inertia and m_v the vehicle mass. The stiffness elements are transmission input shaft, forward sun shaft, output shaft, propeller shaft, gear meshes, axles and tires. The second gear transmission speed ratio is selected as $n_T = r_4/r_3 = 1.47$ and the final drive ratio as $n_F = r_7/r_6 = 3.45$. The model is described with torsional finite elements and the generalised global coordinate vector $\boldsymbol{\theta} = \{\theta_1 \ldots \theta_{10}\}^{\mathrm{T}}$. The system is assembled given stiffness connections such as k_2 (shaft) and k_3 (geared):

$$\boldsymbol{\theta}_{e2} = \begin{Bmatrix} \theta_2 \\ \theta_3 \end{Bmatrix}, \ \mathbf{I}_{e2} = 0.5\mathrm{diag}[J_2 \ J_3], \ \mathbf{K}_{e2} = \begin{bmatrix} k_2 & -k_2 \\ -k_2 & k_2 \end{bmatrix}, \tag{13a–c}$$

$$\boldsymbol{\theta}_{e3} = \begin{Bmatrix} \theta_3 \\ \theta_4 \end{Bmatrix},\ \mathbf{I}_{e3} = 0.5\mathrm{diag}[J_3\ J_4],\ \mathbf{K}_{e3} = \begin{bmatrix} r_3^2 k_3 & -r_3 r_4 k_3 \\ -r_3 r_4 k_3 & r_4^2 k_3 \end{bmatrix}. \tag{14a–c}$$

The reversal of direction of rotation by the gears has been ignored as it is irrelevant to the vibratory system and analysis; in fact, the planetary gear set (except for reverse gear) and final drive do not reverse rotation. In this model, the clearance is applied in two locations, at the transmission mesh between coordinates 3 and 4 ($i = 3$) and at the final drive mesh between coordinates 6 and 7 ($i = 6$). The backlash for the transmission gear pair is set at high values, for the sake of illustration, 2.0 mm and for the final drive gear pair at 4.0 mm, as these values may also be seen as inclusive of nearby lashes from the splines and joints. The global system is of the form:

$$\mathbf{I}\ddot{\boldsymbol{\theta}} + \mathbf{C}\dot{\boldsymbol{\theta}} + \mathbf{K}(\theta)\boldsymbol{\theta}(t) = \mathbf{T}(\theta, \dot{\theta}, t), \tag{15}$$

$$\mathbf{I} = \mathrm{diag}[J_1 \ldots J_{10}], \tag{16}$$

$$\mathbf{K} = \begin{bmatrix}
k_1 & -k_1 & & & & & & & & \\
-k_1 & k_1+k_2 & -k_2 & & & & & & & \\
 & -k_2 & k_2+r_3^2k_3 & -r_3r_4k_3 & & & & & & \\
 & & -r_3r_4k_3 & r_4^2k_3+k_4 & -k_4 & & & & & \\
 & & & -k_4 & k_4+k_5 & -k_5 & & & & \\
 & & & & -k_5 & k_5+r_6^2k_6 & -r_6r_7k_6 & & & \\
 & & & & & -r_6r_7k_6 & r_7^2k_6+k_7+k_9 & -k_7 & -k_9 & \\
 & & & & & & -k_7 & k_7+k_8 & & -k_8 \\
 & & & & & & -k_9 & & +k_9+k_{10} & -k_{10} \\
 & & & & & & & -k_8 & -k_{10} & k_8+k_{10}
\end{bmatrix}. \tag{17}$$

The stiffness matrix is tri-diagonal apart from the driveline subsystem, here there is branching at the final drive output and a tire stiffness coupling left and right wheel hubs to the same tire/vehicle coordinate.

5.2. Modal analysis of the linear system

The eigensolutions are found for Eq. (15) with $\mathbf{T} = 0$ and $\mathbf{C} = 0$. There is one zero eigenvalue (rigid body rotation) and 9 non-zero eigenvalues, as given in Table 2. The eigenvector for the rigid body mode, $\boldsymbol{\psi}$, describes the absolute displacements for the transmission in second gear and for final drive gearing. The frequencies and mode shapes of this reduced system match closely with those of the detailed powertrain system. They are compared in Table 2. Note that the forward sun gear/ring gear coordinates from the detailed model are translated to transmission input/output coordinates for comparison. In the model reduction, the combined stiffness elements are summed in series and the lumped masses carefully redistributed to keep the same overall stiffness and inertia. The reduction process has been successful. Only the 'Transmission II', 'Propeller Shaft I' and 'Transmission III' modes have a marked difference in frequency. The mode shapes are very similar for the former two. Interestingly, the 'Transmission III' mode shape has differences in sign, but not in magnitude. These differences at higher frequencies are expected with the reduction process, yet these higher modes could be excited by the transient impacts.

5.3. Construction of the viscous damping matrix

In automotive powertrain systems, nonlinear damping effects are seen but we assume viscous damping and attempt to construct $\mathbf{C}$ with the same form as $\mathbf{K}$. However, damping of the shuffle mode (first mode of

Table 3
Modal damping ratios for the reduced model of the automatic transmission powertrain system

Mode description	Damping ratio (%)	Enhanced damping ratio (%) with dynamic drag 2 N ms/rad
Driveline shuffle	0.6	8.2
Axle left	5.1	5.1
Axle right	5.2	5.2
Transmission and driveline I	3.8	3.8
Transmission and driveline II	2.7	2.7
Transmission I	2.5	2.5
Propeller shaft I	5.4	5.4
Propeller shaft II	1.8	1.8
Transmission III	2	2

vibration) is difficult with application of only viscous damping elements in parallel with stiffness (the Voight Model), without the inclusion of a dynamic model for the torque converter. The viscous damping coefficients as applied yield the damping ratios of Table 3. Observe that all modes are reasonably damped but the damping ratio at the first mode is only 0.6%. Increasing the tire damping or other physical damping elements could further dampen this mode but with the unwanted effect of raising other damping ratios or even overdamping some modes. A viscous damping matrix may be constructed to achieve fixed damping ratios for all modes (such as 5%). This matrix is often fully populated with a combination of negative and positive damping coefficients necessary to achieve high damping at the shuffle mode. For nonlinear simulations, in some instances, this method could cause the system to become numerically unstable, though it is appropriate for a linear time-invariant system. Consequently, to achieve sufficient damping for the first mode, an inertial damping element is applied at turbine as $D_I(\dot{\theta}, t) = -d_1(\dot{\theta}_1(t) - \bar{\dot{\theta}}_1(t))$, where d_1 is the viscous (drag) damping coefficient and $\bar{\dot{\theta}}_1(t)$ is the mean speed of the turbine. For the free vibration analysis of the linearised system, the mean speed is zero and the dynamic drag coefficient shifts into the **C** matrix as a diagonal element. Using $d_1 = 2\,\mathrm{N\,ms/rad}$ increases the first damping ratio to 8.2%, without affecting other modes (Table 3).

5.4. Transient analysis

The system of governing Eq. (15) includes piecewise functions for the stiffness discontinuity, its solutions include the rigid body motion of the powertrain, forced response at lower modes and nonlinear (transient) response. The simulation is programmed in Matlab with ODE15S, a solver that uses Gear's Method for stiff systems [21]. Results were comparable to those obtained via a fourth-order Runge–Kutta solver though the Gear's Method was about 12 times faster. Note the simulated time is 8 s so as to capture the entire driving event, parametric studies would be less than 1 s, providing reasonably efficient computation times. Convergence was studied by doubling and halving the maximum time step and the solutions were practically identical though the high-frequency response after impacts was more accurate for a smaller time increment.

5.5. Torque excitations

Torque excitations include ramped-down engine torque, sharp applications of brake torque and gradual changes in torque at the tires from the changing gradient of incline with respect to the travelling vehicle. Interpolation on an empirical map (for a typical engine) is used to give the engine mean torque, $T_m(\dot{\theta}_1, \eta)$ on solutions for engine speed, $\dot{\theta}_1(t)$, at a given throttle setting, $\eta(t)$. It is applied directly to the combined turbine, engine and flywheel inertia. Throttle setting is initially at $\eta_I = 0.1$ and remains constant until $t(P) = 4\,\mathrm{s}$. Then the throttle is reduced by $\Delta\eta = \eta_i - \eta_f$ over $\Delta t_\eta = t(q) - t(P) = 0.2\,\mathrm{s}$ for $\eta_f = 0.05$. This change in throttle setting

is a sine smoothened ramp-down, as described below:

$$\eta(t) = \begin{cases} \eta_i, & t < t(p), \\ 0.5(\eta_i + \eta_f) + 0.5\,\Delta\eta \sin\left[\dfrac{\pi(t - t(p))}{\Delta t_\eta} + 0.5\pi\right], & t(p) \leqslant t \leqslant t(q), \\ \eta_f, & t > t(q). \end{cases} \tag{18}$$

Torque pulsations are added for a typical six cylinder engine, $N = 6$, i.e. at third, sixth and ninth orders of engine (turbine) speed, $\dot{\theta}_1(t)$, giving, $T_{\text{eng}}(t) = T_m(\dot{\theta}_1, \eta) + \sum_j A_j \sin(j\dot{\theta}_1 t + \phi_j)$, $j = 3, 6, 9$, where $j = 0.5N$, N, $1.5N$ are the dominate torque orders, A_j is the amplitude and ϕ_j is the phase for the jth order.

Second, the brake torque, $T_b(t)$, is applied to simulate a driver pressing once on the brake and releasing, essentially a tap. The driver then presses again and holds constant braking torque. The torque is applied at $t(P) = 4$ s for $\Delta t_{b_1} = t(r)^- - t(p) = 0.5 - \Delta t(r)^-$ (first ramp) and released at $t = t(r)^- = t(r) - \Delta t(r)^-$, which is the time step preceding $t(r)$. Here, $\Delta t(r)^-$ is the step size at $t(r)^-$. The brake torque is applied again at $t(r) = 4.5$ s for $\Delta t_{b_2} = t(s) - t(r) = 0.5$ s (second ramp) and from $t(S)^+ = 5 + \Delta t(s)$ it is held constant at $T_b(s) = 600$ N m. The brake torque is split evenly over left and right hubs. An algorithm is presented below:

$$T_b(t) = \begin{cases} 0, & t < t(p), \\ \dfrac{T_b(s)}{\Delta t_{b_1}}[t - t(p)], & t(p) \leqslant t < t(r), \\ \dfrac{T_b(s)}{\Delta t_{b_2}}[t - t(r)], & t(r) \leqslant t \leqslant t(s), \\ T_b(s), & t > t(s). \end{cases} \tag{19}$$

Third, the road profile is modelled with a parabolic curve which describes a hill of width, $w = 100$ and height, $h = 5$. The path of the vehicle along the equation of the curve is determined dynamically from the absolute angular displacement of the tire, $\theta_{10}(t)$, without any slip. Using x and y as the respective vehicle longitudinal and vertical positions on the hill, the equation of the curve, gradient and domain for the hill are $y = h - (4h/w^2)x^2$, $(\mathrm{d}y/\mathrm{d}x) = -(8h/w^2)x$ and $x \in \{-0.5w\ 0.5w\}$. Initially, at $t(0)$, the vehicle longitudinal position, tire angular displacement and road gradient are $x(0) = -0.5w$, $\theta_{10}(0) = 0$, $\chi(0) = -(8h/w^2)x(0)$. This initial road gradient is a maximum and equal to 11.46° for the given h and w. At each time step, t_k, the longitudinal position is determined by the following, where $\chi(t) = -(8h/w^2)x(t)$, $x(t_k) = x(t_{k-1}) + r_{\text{tire}} \cos\chi(t_{k-1})[\theta_{10}(t_k) - \theta_{10}(t_{k-1})]$. Values of $x(t_k)$ and $\chi(t_k)$ are stored at each step and used as $x(t_{k-1})$ and $\chi(t_{k-1})$ in the subsequent time steps. The time-varying torque on the tire from the weight of the vehicle is determined given the tire radius, vehicle mass and road gradient, $T_{\text{grad}}(t) = r_{\text{tire}} m_v g \sin\chi(t)$. Finally, a constant $D_v = 30$ N m is applied at the tire representing both aerodynamic drag and rolling resistance since the vehicle speed is fairly constant. The global torque vector for Eq. (15) may be written as follows given the above descriptions, also torque offsets Eq. (12) for the clearance algorithm Eq. (11) applied at elements $i = 3$ and 6:

$$\mathbf{T} = [(T_{\text{eng}} - D_t)\ T_{\delta_3}\ T_{\delta_4}\ 0\ T_{\delta_6}\ T_{\delta_7}\ -0.5T_b\ -0.5T_b\ -(T_{\text{grad}} + D_v)]^{\mathrm{T}}. \tag{20}$$

5.6. Initial conditions

First, the system of equations of motion Eq. (15) is sub-structured as follows where $\boldsymbol{\theta}_{\mathrm{a}} = \{\theta_1 \ldots \theta_9\}$ and $\boldsymbol{\theta}_{\mathrm{b}} = \{\theta_{10}\}$:

$$\boldsymbol{\theta} = \{\boldsymbol{\theta}_a | \boldsymbol{\theta}_b\}^{\mathrm{T}};\ \mathbf{I} = \begin{bmatrix} \mathbf{I}_a & \mathbf{I}_{ab} \\ \mathbf{I}_{ba} & \mathbf{I}_b \end{bmatrix};\ \mathbf{K} = \begin{bmatrix} \mathbf{K}_a & \mathbf{K}_{ab} \\ \mathbf{K}_{ba} & \mathbf{K}_b \end{bmatrix};\ \mathbf{C} = \begin{bmatrix} \mathbf{C}_a & \mathbf{C}_{ab} \\ \mathbf{C}_{ba} & \mathbf{C}_b \end{bmatrix};\ \mathbf{T} = [\mathbf{T}_a | \mathbf{T}_b]^{\mathrm{T}}. \tag{21a–d}$$

Then initial condition displacements are found for the grounded system as follows, note that gears are in mesh so values of T_{δ_i} are zero:

$$\boldsymbol{\theta}_a(0) = \mathbf{K}_a^{-1}(-\mathbf{I}_a \ddot{\boldsymbol{\theta}}_a(0) + \mathbf{T}_a(0)), \quad \boldsymbol{\theta}_b(0) = 0, \tag{22a,b}$$

where the rigid body accelerations are given by $\ddot{\boldsymbol{\theta}}_a(0) = \ddot{\theta}_1(0)\boldsymbol{\psi}_a$ and $\boldsymbol{\psi}_a$ is sub-structure a of the eigenvector, $\boldsymbol{\psi}$, of rigid body motion (Table 2), normalised to $\psi_1 = 1$ (turbine coordinate), that corresponds with the zero eigenvalue from the homogeneous system of Eq. (15). The turbine acceleration is determined with the system considered as one lumped equivalent inertia $\ddot{\theta}_1(0) = I_{\text{eqv}}^{-1}(T_{\text{eng}}(0) - (\varphi_{10}/\varphi_1)[T_{\text{grad}}(0) + D_v(0)])$. Note that $\varphi_1/\varphi_{10} = n_T n_F$ is the speed ratio between the engine and the tire. Also, the system equivalent inertia with respect to the turbine coordinate is $I_{\text{eqv}} = \sum_{1:m}^{m=10}[\mathbf{I}(m,m)(\varphi_m/\varphi_1)^2]$. Similarly φ_1/φ_m is the effective speed ratio between the turbine and any coordinate m. Engine initial angular velocity is prescribed as $\dot{\theta}_1(0) = 220$ rad/s, then for all coordinates the initial condition velocities are, $\dot{\boldsymbol{\theta}}(0) = \dot{\theta}_1(0)\boldsymbol{\psi}$. The initial condition displacements given by Eq. (22) are for a linearised stiffness matrix with respect to the nonlinear stiffness for clearance, accordingly a displacement offset is applied to account for the torque offsets within the torque vector Eq. (20). First, the coordinates upstream of the transmission gear mesh ($i = 3$) are rotated through half the transmission clearance and half the final drive clearance (accounting also for the transmission ratio):

$$\hat{\theta}_1(0) = \theta_1(0) + \frac{\delta_3}{2r_3} + n_T\frac{\delta_6}{2r_6},\ \hat{\theta}_2(0) = \theta_2(0) + \frac{\delta_3}{2r_3} + n_T\frac{\delta_6}{2r_6},\ \hat{\theta}_3(0) = \theta_3(0) + \frac{\delta_3}{2r_3} + n_T\frac{\delta_6}{2r_6}. \quad (23a-c)$$

Then coordinates upstream of the final drive gear mesh ($i = 6$) are rotated through half the final drive clearance:

$$\hat{\theta}_4(0) = \theta_4(0) + \frac{\delta_6}{2r_6},\ \hat{\theta}_5(0) = \theta_5(0) + \frac{\delta_6}{2r_6},\ \hat{\theta}_6(0) = \theta_6(0) + \frac{\delta_6}{2r_6}. \quad (24a-c)$$

The initial condition vectors for the nonlinear transient analysis are then constructed from Eq. (22a,b) and the initial angular velocity vector with adjusted values Eq. (23,24) replacing respective values in Eq. (22a)

5.7. Two simulation studies

First consider the damping ratios of Table 3, the first mode damping ratio at 8.2% gives a reasonable assumption for damping in an automatic transmission powertrain with open torque converter. For this simulation, component speeds are shown in Fig. 9. The engine, transmission and vehicle speeds reduce slightly as the vehicle is driven up the crest and at around $t = 4$ s the road gradient changes from positive to negative and the driver releases throttle to practically zero engine torque. Shortly afterwards the brake is tapped and held on. Evident in Fig. 9, from $t = 4.5$ to 4.75 s, are the gear impacts in the transmission and final drive. Relative displacements in the shafting (Figs. 10 and 11) show the rigid body and transient motion of the driving system, as well as the responses from engine firing (visible in Fig. 10 around $t = 4$–4.05 s). As the car rises the crest, the twist gradually reduces in line with reducing gradient load (though these first 4 s are not shown in the plot). The change in torque is large but the time is long so there is no transient vibration. From

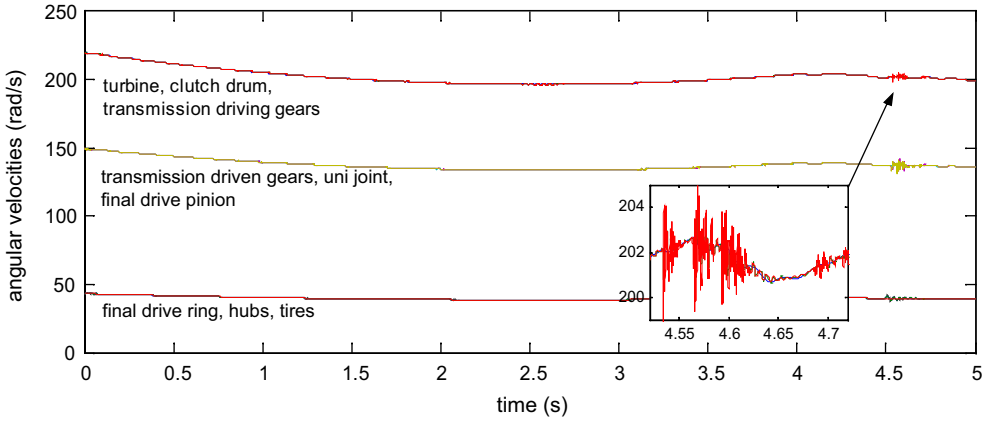

Fig. 9. Simulated component speeds with high dynamic drag damping in the turbine.

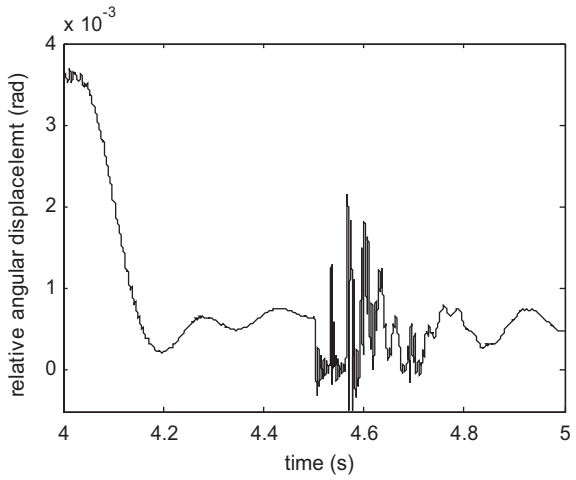

Fig. 10. Simulated input shaft twist with high dynamic drag damping in the turbine.

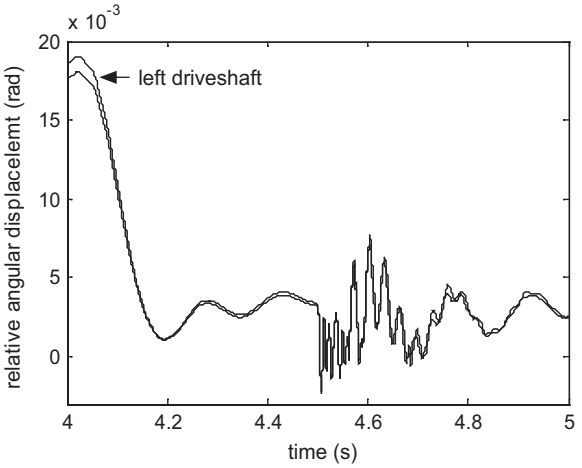

Fig. 11. Simulated driveshaft (axle) twist with high dynamic drag damping in the turbine.

$t = 4$ to 4.2 s the engine torque reduces. This is enough time for a cycle of the first mode so some of the response is already decaying before the engine torque drop is complete. Meanwhile the solution mostly follows the path of rigid body motion. This shows that the damping of the shuffle mode has some significant effect on the occurrence of the first gear impact as long as the engine transient excitation is not very abrupt (in time). For a true step-down in torque, it will have little effect for the first cycle of response and hence little effect on the gear impacts [10]. The nature of the engine transient torque is critical in the response. So is the shaping of the resulting torque transient through the system before reaching the appropriate clearances; this shape is affected by stiffness and damping. For this driving situation, the response plots show that there are no gear impacts purely from the engine torque transient. This is because the mean load was still sufficiently high and the transient vibration not large enough for gear separation. This does not discount the typical relationship between 'shuffle' and 'clunk' in vehicles which we know can occur from large torque rise/fall events under the presence of low mean load (especially with light damping such as in manual transmission powertrains). In this instance the gear impacts and resulting impulsive responses would not have occurred had it not been for the transient braking torque adding further oscillations and variation in rigid body motion (static twist). The three clear tooth separations and subsequent single-sided impacts shown in Fig. 12 (transmission) and Fig. 13 (final drive) occur almost immediately after the brake release ($t = 4.5$ s). This release excites the system as

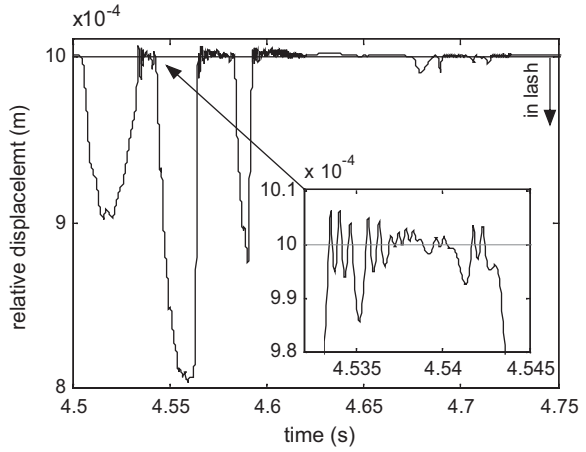

Fig. 12. Simulated mesh displacement in the transmission with high dynamic drag damping in the turbine.

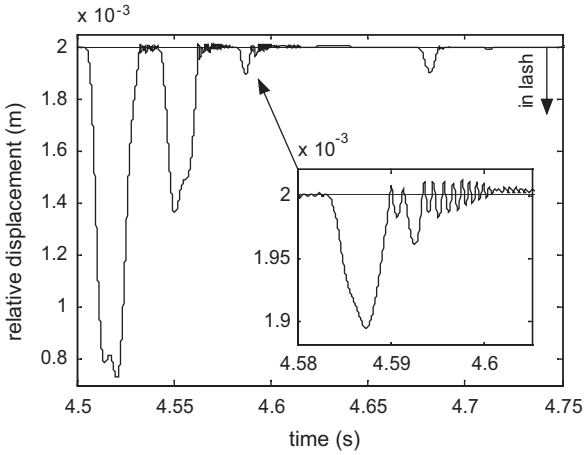

Fig. 13. Simulated mesh displacement in the final drive with high dynamic drag damping in the turbine.

a step-down event. The three tooth separations have roughly the frequency of the axle mode (around 30 Hz). Referring to the normalised modes of Table 2; the step-down torque directly excites the axle mode with maximum effect as applied at the wheel hubs (brake rotor). Hence, the impacts resulted mainly from the braking transient exciting the axle modes. However, other transients and mean load (or a lack of) also contributed. The minor impacts after $t = 4.67$ s are due to the excited axle modes and more significantly due to the 'shuffle' vibrations that originated from the engine transient; these are further excited by the braking transient. We see this from a second simulation run with the dynamic drag on the turbine reduced for a lowest mode damping ratio of 2.5%. Figs. 14 and 15 show the resulting relative displacements for the transmission and final drive. Up to $t = 4.67$ s the result is much the same in terms of the nature and number of impacts. This is as the change in rigid body motion from the braking transients and the axle mode vibrations (unchanged by the torque converter drag damping) were the chief causes of gear separation. However, the second simulation clearly has more impacts on the later cycles of shuffle response ($t = 4.65$–4.75 s), given the smaller damping for the lowest mode. The difference in this particular simulation is not great, 'shuffle' is not the main cause of the gear impacts in the first case and this similarity illustrates that. Finally, the effect of engine torque pulsations were examined with the amplitudes of oscillations doubled and halved. As expected, no significant effects on transient impacts are seen. Consequently, only the true transient excitations must be considered for impulsive studies.

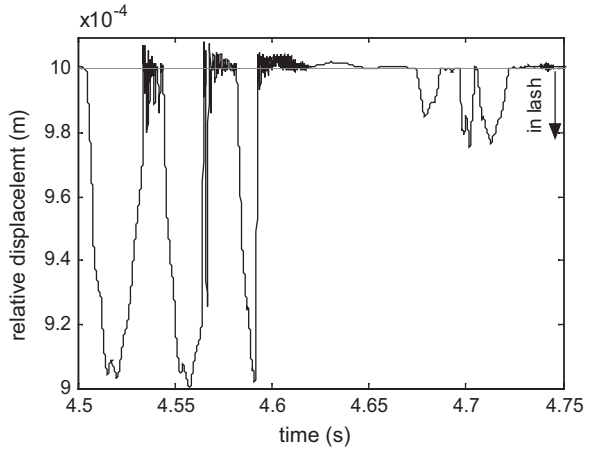

Fig. 14. Simulated mesh displacement in the transmission with low dynamic drag damping in the turbine.

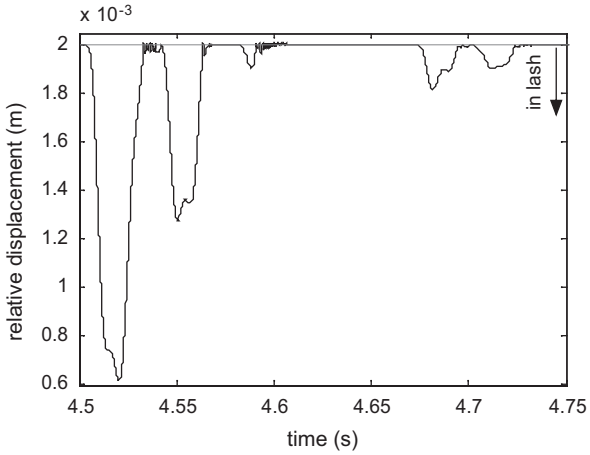

Fig. 15. Simulated mesh displacement in the final drive with low dynamic drag damping in the turbine.

6. Experimental study

6.1. Test rig, free vibration experiment and system model

The powertrain test rig of Fig. 2 includes all the components of the vehicle powertrain and has been designed to simulate a vehicle mass of 1500 kg via a flywheel system. A set of locomotive wheels provide the inertia to simulate this mass and are mounted so as to be driven by the tires. The load from aerodynamic drag and any road gradient can be applied to the test rig via the flywheel system. Test rig parameters for inertia, stiffness and gear dynamics are determined from detail drawings and measurements of the components. Parameters that are difficult to determine include tire stiffness, clutch and band friction characteristics, torque converter output torque and system damping, to name some. An experiment was developed to simultaneously excite low-frequency free vibration of the vehicle driveline and high-frequency transient vibration from impacts. On the test rig, the automatic transmission is placed in park (grounding the rigid body motion). To apply the load a 'torsion bar' has been rigidly attached to each wheel rim (Fig. 16). An electromagnetic release mechanism is attached to the end of the torsion bar. On each side up to 20 kg of mass is evenly loaded onto the bar via the electromagnets. Turning off the power to the electromagnets releases the weights, freeing the stored potential energy. (The masses are dropped onto thick rubber pads to minimise vibration transmitted through the floor and test beds to the powertrain system.) The loading twists the driveline from the wheels up to the

Fig. 16. Torsion bar for free vibration experiment.

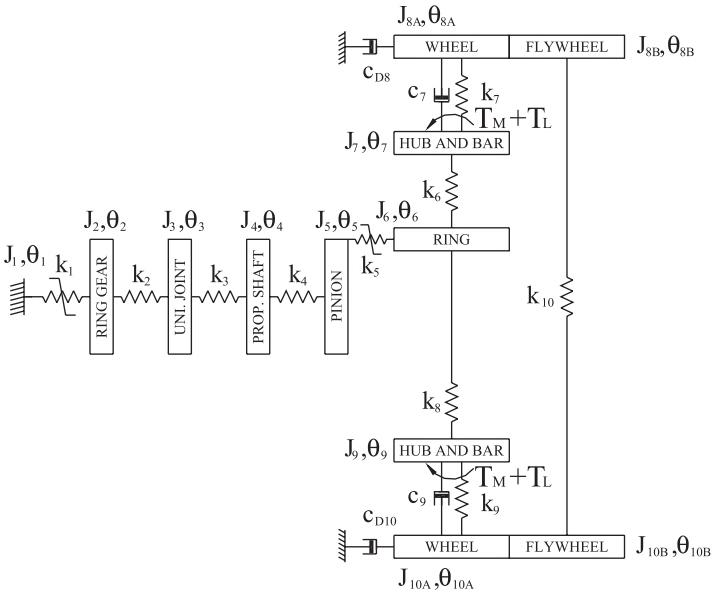

Fig. 17. Reduced order torsional model for driveline free vibration experiment.

parking pawl; potential energy is stored in the overall compliance. Accelerometers and strain gauges measure the free vibration response. Data acquisition is triggered from an accelerometer located at the end of the bar. Three sets of experiments are conducted as described in the subsequent sections.

A reduced order dynamic model is developed for the drivetrain sub-system (Fig. 17). This model is grounded where the parking pawl mechanism holds the ring gear (output gear) of the automatic transmission. The propeller shaft is discretised into two torsional springs. The final drive and differential is reduced to a simple gear pair. The inertia and stiffness parameters were carefully determined from drawings and measurements. The parking pawl stiffness and gear mesh stiffness are assumed as 2×10^8 and 5×10^8 N/m, respectively. For transient free vibration the torque vector includes the applied torque at the hub coordinates; the sum of mean load from the electromagnet and overhanging torsion bar (T_M) and the load to be released for the particular experiment (T_L). The clearance type algorithm is used for the parking pawl and final drive stiffness elements. Initial condition velocities are all zero, initial condition displacements are $\boldsymbol{\theta}_0=\mathbf{K}^{-1}\mathbf{T}_0$, where $\mathbf{T}(t)=[0\ 0\ 0\ 0\ 0{-}(T_M+T_L)\ 0\ {-}(T_M+T_L)\ 0]^{\mathrm{T}}$ is the torque vector at $t(0)$. The angular displacements need to be adjusted for gear lash, δ_i, in a similar fashion to the reduced order automatic transmission model. Matlab solvers are used for simulation too with a maximum time step of 0.0001 s. At $t=0^+$ the applied load is removed ($T_L=0$) initiating transient vibration though the mean load stays applied. The lowest mode of the

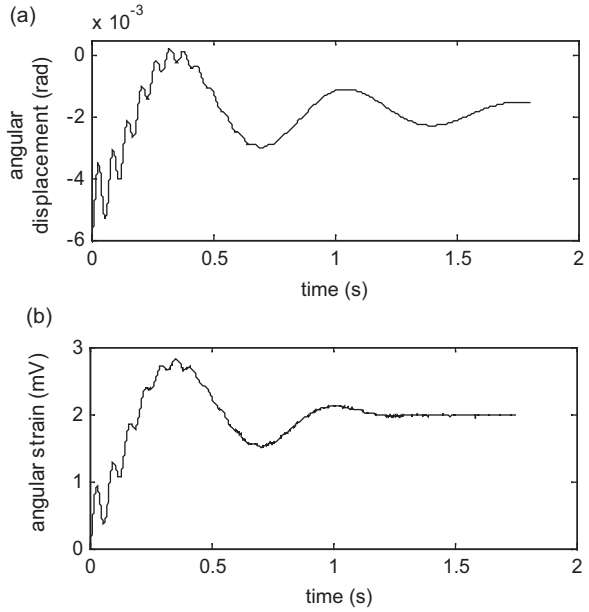

Fig. 18. Mass release experiment I: left axle time history comparison for simulation (a) and test (b).

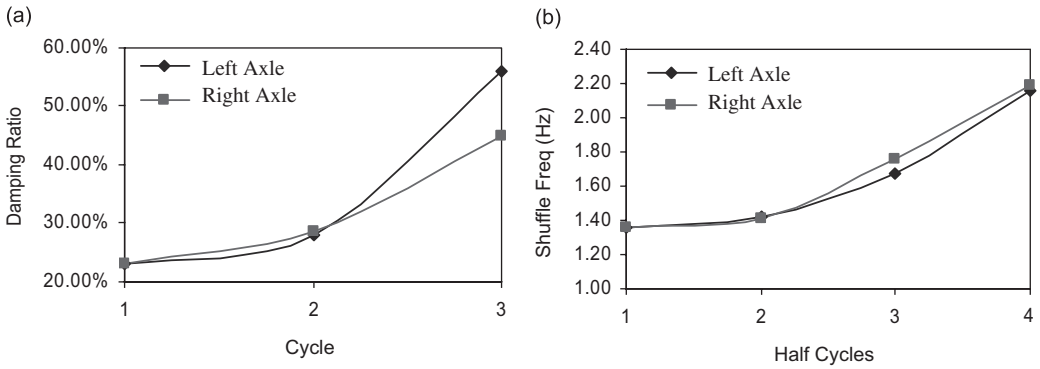

Fig. 19. Mass release experiment I: (a) damping of first mode vs. cycles and (b) first mode frequency vs. half cycles.

driveline system is 1.44 Hz followed by axle modes, which at 17.1 and 17.6 Hz are significantly different to those shown for the previous models. In the absence of the large inertia of the torsion bar and electromagnet (mass removed from the hub coordinate) these modes would shift back to about 32–33 Hz.

6.2. *Results for Experiment I—mass release with no clunk*

The applied load for this experiment is approximately 5 kg on each side. Fig. 18b provides the time domain results for the left axle twist. The strain is measured in mV and the signal is offset for zero values at the initial load. For this experiment the driveline 'shuffle' frequency and damping ratio are investigated. Clearly visible in the result are the axle modes at around 16–17 Hz. They have approximately a 5% damping ratio. The drag torque on the tire and flywheel subassembly has been found to be the significant factor for damping the 'shuffle' mode. For the results (both left and right axles) the frequency has been calculated across each cycle and damping ratio across each half cycle. The variation over cycles is shown in Figs. 19. At the end of the third cycle the system is basically motionless. This third cycle is not visible in the plot. We believe the nonlinear nature can be attributed to the rolling friction. The damping is difficult to determine accurately given the nature of this experiment. A linear simulation is performed to match this result with viscous damping included

in the tire to achieve a damping ratio for the axle modes of 5%. This damping element takes the 'shuffle' damping ratio to only 0.3%. This shows that the tire is not the significant contributor to the 'shuffle' mode damping as discussed in the nonlinear simulation for the typical driving situation (Section 5). A small value of viscous damping is included in all other shaft elements. A constant value for viscous inertial damping of 400 N ms/rad is applied at the tires, taking the damping ratio to 14%, which extrapolating out from Fig. 19a for the larger load of experiment 2 (more cycles) is reasonable. Note that this damping parameter is added only to the diagonal of the damping matrix. Fig. 18 provides the results for the simulation compared with the experiment, for the left axle. No attempt has been made to match amplitude of strain readings to angular displacement. As can be seen from the figure, the dynamic model and simulation accurately captures the 'linear' response. As the cycles progress the actual damping may increase as shown in Fig. 19a, from 1.0 s onwards there is no longer good comparison using the linear simulation. The result confirms the linear dynamic model up to this point.

6.3. Result for Experiment II—mass release with clunk

When the larger load is applied (20 kg each side), the response of the system features the nonlinear tooth impacts. The final drive lash was measured as 1.1° at the input (ring gear) which would include clearances between ring and pinion, in the differential gears and in splines. The lash at the parking pawl mechanism is significantly larger, it was measured as 3.6° which translates to 3.8 mm at the circumference of the transmission ring gear. Both measurements were made within $\pm 0.1^\circ$ accuracy. Using these backlash values and the pre-determined damping values (from Experiment I) the nonlinear simulation was run and compared with the Experiment II results. Fig. 20 compares the output shaft twist as measured strain to predicted angular displacement. Experiment II and simulation compare well for the first 1.4 s of oscillations. The left and right hand axle twist is similarly well matched. Fig. 21 gives displacements across the clearance for the parking pawl and final drive (for the simulation) and shows a single-sided impact transient response. In the experiment the clearance is entered on the second cycle of response. This is not captured by the numerical simulation. Adjustments to the size of lash, absolute damping, mean or applied load and stiffness have been made in simulations but no improvement was seen; the measured values are provided as they are good results up to 1.4 s. Tweaking these measurements also provides no improvement. The discrepancy in the result after 1.4 s

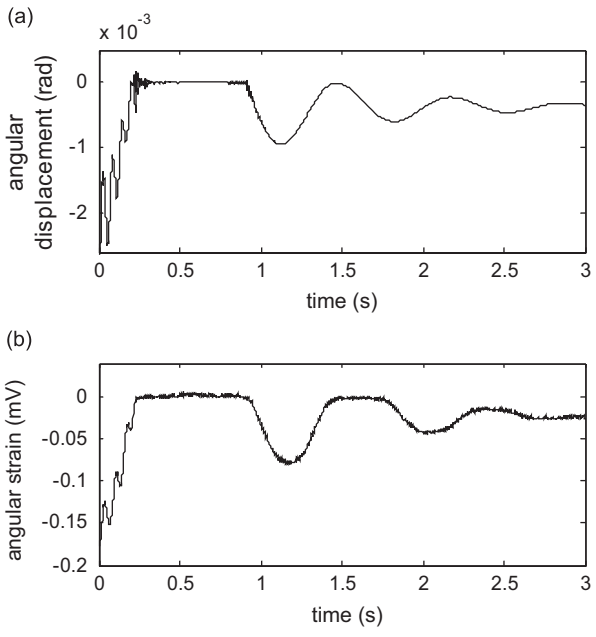

Fig. 20. Mass release experiment II: output shaft time history comparison for simulation (a) and experiment (b).

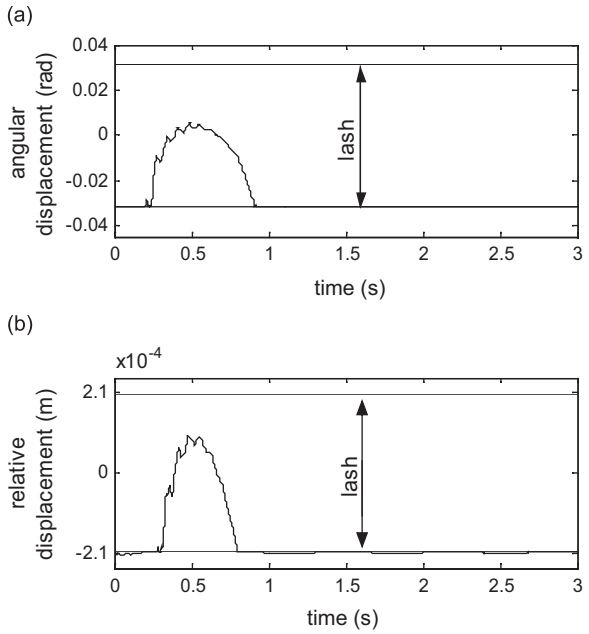

Fig. 21. Mass release experiment II: simulation time history for gear separation—parking pawl (a) and final drive (b).

can be attributed to the nonlinear damping, additional lash locations from splines and universal joints or nonlinear tire stiffness. However, the results confirm the system parameters for overall inertia, stiffness and the measured lash.

6.4. Result for Experiment III—rocking test

Fig. 22a provides an example of the characteristics of double-sided impacts receding to single-sided impacts as measured strain in the right axle. To obtain this result the driveline is simply rocked by hand on each side with the torsion bar and data sampled after the rocking has stopped. The flat sections show the system passing through lash, where the strain is zero. The sinusoidal 'humps' are the driveline twist when the lash is closed. The humps occur on each side (top and bottom) of the flat section for double-sided impacts and just on one side for single-sided impacts. One side has a larger response due to the presence of the mean load from the combined moment of the torsion bar and electromagnet mass. Fig. 22b gives corresponding measured data for an accelerometer mounted on the propeller shaft to pick up tangential acceleration in the transverse plane. The data is clipped but shows clearly the high frequency transients during the impact events (the corners of the flat sections for angular strain).

7. Conclusion

This study has made several contributions to understanding of impulsive responses in automatic transmission systems with multiple clearances under transient excitations. (1). A detailed model was formulated including the derivation of matrix elements for planetary and final drive gear sets. (2). A reduced order system was formulated yielding a tractable nonlinear problem. Application of damping, transient torques, mean loads, dynamic torque converter drag and determination of appropriate initial conditions are all important aspects of the problem. A typical driving situation (with respect to road conditions and driver behaviour) was successfully simulated and is readily adaptable to practical transient gear impact (clunk) problems. It has been shown that only transient loads should be considered as the pulsating torque from the engine (that could excite the gear rattle) was found to have no effect, these items have not been previously reported. (3). An experiment was performed to verify the proposed approach. Parameters (inertia, stiffness,

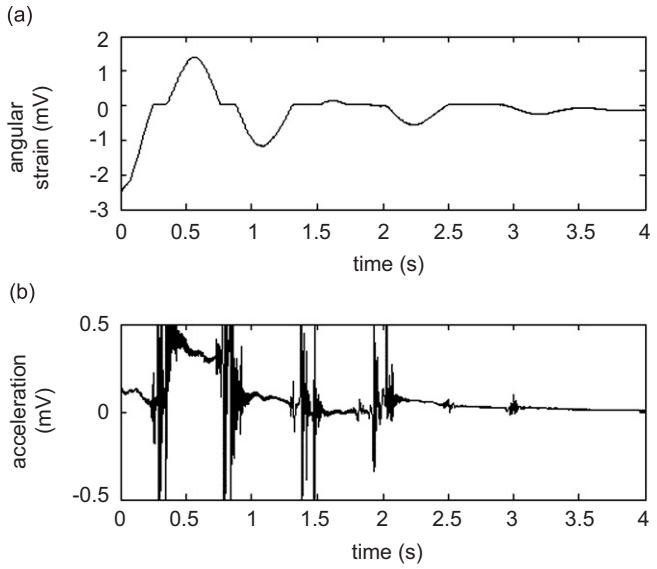

Fig. 22. Experiment III: double and single-sided impacts excited by rocking the torsion bar—measured angular strain (a) and pinion nose acceleration (b).

damping and backlash) were successfully identified and the nonlinear response under free vibration of the driveline sub-system was duplicated. Finally, our results demonstrate characteristics similar to those of previous experiments and simulations [10,12]. See Ref. [10] and compare results with Fig. 22a for strain measurements; further, see Ref. [12] and compare their results with Fig. 22b for acceleration spikes. In our current work no attempt has been made to quantify magnitude of impact responses as evaluations of appropriate metrics have been made in a subsequent paper [22].

Acknowledgements

Financial support for part of this research is provided jointly by the Australian Research Council (Grant no. C00107787), the University of Technology, Sydney, Australia and ION Automotive Systems, Sydney, Australia.

References

[1] J. Wang, R. Li, X. Peng, Survey of nonlinear vibration of gear transmission systems, *Applied Mechanics Review* 56 (3) (2003) 309–329.
[2] R.J. Comparin, R. Singh, An analytical study of automotive neutral gear rattle, *ASME Journal of Mechanical Design* 112 (1990) 237–245.
[3] T.E. Rook, R. Singh, Dynamic analysis of a reverse–idler gear pair with concurrent clearances, *Journal of Sound and Vibration* 182 (2) (1995) 303–322.
[4] A. Kahraman, G.W. Blankenship, Interaction between external and parametric excitations in systems with clearance, *Journal of Sound and Vibration* 194 (1996) 317–336.
[5] A. Kahraman, G.W. Blankenship, Experiments on nonlinear dynamic behavior of an oscillator with clearance and time-varying parameters, *ASME Journal of Applied Mechanics* 64 (1997) 217–226.
[6] G.W. Blankenship, A. Kahraman, Steady state forced response of a mechanical oscillator with combined parametric excitation and clearance type nonlinearity, *Journal of Sound and Vibration* 185 (1995) 743–765.
[7] R. Singh, H. Xie, R.J. Comparin, Analysis of automotive neutral gear rattle, *Journal of Sound and Vibration* 131 (2) (1989) 177–196.
[8] C. Padmanabhan, R.C. Barlow, T.E. Rook, R. Singh, Computational issues associated with gear rattle analysis, *ASME Journal of Mechanical Design* 117 (1995) 185–192.
[9] T.C. Kim, T.E. Rook, R. Singh, Effect of smoothening functions on the frequency response of an oscillator with clearance non-linearity, *Journal of Sound and Vibration* 263 (3) (2003) 665–678.
[10] R. Krenz, Vehicle response to tip-in/tip-out, SAE Technical Paper 850967, 1985, SAE Publications Website: 〈www.sae.org/technical/papers/850967〉.

[11] Ph. Couderc, J. Callenaere, J. Der Hagopian, G. Ferraris, Vehicle driveline dynamic behavior: experiment and simulation, *Journal of Sound and Vibration* 218 (1) (1998) 133–157.
[12] J.W. Biermann, B. Hagerodt, Investigation of the clonk phenomenon in vehicle transmissions—measurement, modelling and simulation, *Proceedings of the Institution of Mechanical Engineers Part K: Journal of Multibody Dynamics* 213 (1999) 53–60.
[13] Th. Schumarcher, J.W. Biermann, N. Jansz, J. Willey, K. Küpper, Load change reactions of passenger cars: method of investigation and improvement, *Proceedings of the Institution of Mechanical Engineers, Part K: Journal of Multibody Dynamics* 217 (2003) 283–291.
[14] M.T. Menday, H. Rahnejat, M. Ebrahimi, Clonk: an onomatopoeic response in torsional impact of automotive drivelines, *Proceedings of the Institution of Mechanical Engineers, Part D: Journal of Automobile Engineering* 213 (1999) 349–357.
[15] A. Farshidianfar, M. Ebrahimi, H. Bartlett, Hybrid modelling and simulation of the torsional vibration of vehicle driveline systems, *Proceedings of the Institution of Mechanical Engineers, Part D: Journal of Automobile Engineering* 215 (2001) 217–229.
[16] S. Theodossiades, M. Gnanakumarr, H. Rahnejat, M. Menday, Mode identification in impact-induced high frequency vehicular driveline vibrations using an elasto-multibody-dynamics approach, *Proceedings of the Institution of Mechanical Engineers, Part K: Journal of Multibody Dynamics* 218 (2004) 81–94.
[17] N. Zhang, A. Crowther, D.K. Liu, J. Jeyakumaran, A finite element method for the dynamic analysis of automatic transmission gear shifting with a 4DOF planetary gearset element, *Proceedings of Institution of Mechanical Engineers, Part D: Journal of Automobile Engineering* 217 (2003) 273–461.
[18] J.-S. Wu, C.-H. Chen, Torsional vibration analysis of gear-branched systems by finite element method, *Journal of Sound and Vibration* 240 (1) (2001) 159–182.
[19] A. Kahraman, Free vibration characteristics of compound planetary gear sets, *Mechanisms and Machine Theory* 36 (2001) 953–971.
[20] A.R. Crowther, N. Zhang, Torsional finite elements and non-linear numerical modelling in vehicle powertrain dynamics, *Journal of Sound and Vibration* 284 (3-5) (2005) 825–849.
[21] L.F. Shampine, M.W. Reichett, The matlab ODE suite, *SIAM Journal of Scientific Computing* 18 (1997) 1–22.
[22] A.R. Crowther, C. Janello, R. Singh, Quantification of impulsive phenomena in torsional systems with clearances, *Journal of Sound and Vibration*, in press, doi:10.1016/j.jsv.2007.05.055.